Robotica (2018) volume 36, pp. 187–203. © Cambridge University Press 2017
doi:10.1017/S0263574717000236

Kinematic analysis and multi-objective optimization of a new reconfigurable parallel mechanism with high stiffness

Guanyu Huang, Sheng Guo, Dan Zhang*, Haibo Qu and Hongyan Tang

Department of Mechanical Engineering, Beijing Jiaotong University, Beijing, 100044, P.R. China
E-mails: huangguanyu0@163.com, shguo@bjtu.edu.cn, hbqu@bjtu.edu.cn, 14116352@bjtu.edu.cn

(Accepted April 22, 2017. First published online: May 30, 2017)

SUMMARY
This paper presents a novel reconfigurable parallel mechanism, which can serve as a machine tool. The proposed parallel mechanism can change its structure parameters by driving a bevel gear system fixed in the base platform. First, the forward and inverse kinematics of the proposed mechanism are investigated. Second, the reachable workspace and Jacobian matrix are conducted. Based on the Jacobian matrix, the stiffness model and dexterity of the end effector are developed in detail. Finally, a multi-objective optimization is performed by using the Genetic Algorithm, and the workspace and global performance indexes of stiffness as well as the dexterity are considered as the performance indices to improve the performance of the reconfigurable parallel mechanism. Finally, Pareto frontier figure and several tables are provided to illustrate the results of the optimization. The results showed the proposed method has improved the performance of the reconfigurable machine tool in terms of its stiffness and dexterity.

KEYWORDS: Reconfigurable parallel mechanism, Kinematic analysis, Jacobian matrix, Stiffness, Multi-objective optimization.

1. Introduction

Parallel robotic systems in contemporary manufacturing operations have challenges meeting the rapidly increasing demands on task adaptability and flexibility in manufacturing. To satisfy the requirements, a number of reconfigurable parallel mechanisms have been proposed, which can rapidly change its structure in terms of hardware and software components.[1−3] Compared with the six degree-of-freedom (DOF) reconfigurable parallel mechanisms, the three-DOF parallel mechanisms have attracted more researchers' attention because six-DOF motions are not always needed in industry. The same as six-DOF parallel mechanism, a three-DOF parallel mechanism has the advantages over its serial counterpart, such as high structural rigidity, high accuracy, and low inertia.[4,5]

Due to the advantages of reconfigurable parallel mechanisms, some scholars have done research in this area. Generally, there are two ways to achieve different configurations, one is to change the number or the topology of limbs[6−8] and the other is to change the structural characteristics.[9,10] In the aspect of mechanism structure, Kong[7] investigated the operation modes of a 3-RER (a serial kinematic chain composed of a revolute (R) joint, a planar (E) joint, and an R-joint) parallel mechanism which can change its configurations to switch from one operation mode to another by changing the topology of each limb. Ye *et al.* [11] presented a diamond kinematotropic chain to reconfigure the constructions of a new family of parallel mechanisms by providing the constraint forces or couples based on the screw theory. Sixteen reconfigurable limbs had been constructed by Ye [11] were presented in the paper. Prior to Ye [11], Azulay *et al.* [12] presented several 3 X PPRS (prismatic-prismatic-revolution

* Corresponding author. E-mail: 14116353@bjtu.edu.cn

https://doi.org/10.1017/S0263574717000236 Published online by Cambridge University Press

sphere) reconfigurable parallel mechanisms by changing the structural characteristics, which had both high static and dynamic stiffness.

For a reconfigurable parallel mechanism, it can reconfigure its architectures to get different kinematic properties, so the kinematic property is the important aspect of reconfigurable parallel mechanism. Many researches in the kinematics of parallel mechanisms have been investigated.[13−18] Gan *et al.* [18] proposed a novel three-DOF parallel mechanism with a reconfigurable joint based on the screw theory, and both forward and inverse kinematics analysis of the 3rTP*S* (hooke-prismatic sphere) parallel mechanism have been obtained and validated by some numerical examples.

In order to evaluate the performance of a parallel mechanism, some criterions have been proposed.[19−24] Xie [21] proposed the indices that assimilate motion/force transmissibility to evaluate the performance of a three-DOF parallel mechanism with redundant joints. Liu [25] proposed a new methodology for evaluating the general parallel mechanisms. Both Xie and Liu presented some useful indices to evaluate the performance of parallel mechanisms, then, the optimal mechanisms can be obtained based on these indices. In general, stiffness is the most significant index in designing and analyzing machine tools. Optimization plays an important role in mechanism design, and it is used to improve the mechanisms performances based on the performance indices.[4,26−28].

However, some reconfigurable parallel mechanisms can reconfigure themselves by changing their DOFs. In contrast to the metamorphic mechanism system, the parallel mechanisms with a continuous adjustable mechanical system have greatly captured the attention from researchers due to their perfect flexibility. Nevertheless, only the workspace and optimization analyses of the reconfigurable mechanisms are insufficient, and some new criteria need to be presented to improve the mechanism performances.

In this paper, a novel continuous reconfigurable parallel mechanism is proposed, which can serve as a machine tool. One of the main features is that the presented mechanism is reconfigurable and it has a middle platform. In order to reconfigure its structure, a bevel gear train is designed and attached to the fixed platform. All the adjustable limbs are connected to the middle platform. With these properties, it is envisioned to be used as a machine tool. This paper is organized as follows. In Section 2, architecture description is presented and mobility is also analyzed. The kinematic analysis is established in Section 3. The working performances are evaluated in Section 4. Finally, the multi-objective optimization process is conducted in Section 6.

2. Design Description

2.1. Architecture description

Figure 1 shows the schematic of the proposed reconfigurable parallel mechanism. This mechanism consists of one fixed and two moving platforms, and the bottom one is the end effector. Between the middle and fixed platforms, there are three limbs which have two revolute joints and two prismatic joints. They are arranged in the order of PRPR (prismatic-revolute-prismatic-revolute) and the first prismatic joint is actuated by the gear train system, and the second prismatic joint is an actuator, which is located between the middle platform and the slider. In order to obtain three DOF, the joints are arranged in the order of PRS (prismatic-revolute-spherical), and the first prismatic joint is actuated. The spindle can hold various tools for drilling, milling, or deburring, etc.

The reconfigurable section is a one-DOF hybrid mechanism, and it is actuated by a gear train system. This central bevel gear drives three other bevel gears, each of which is attached to a swing link that drives slider to deploy the mechanism. In traditional design, the middle platform is always fixed, but in this novel design, the middle platform is connected by three limbs with revolute joints. The new reconfigurable section can create different configurations for the parallel mechanism. In order to keep the stability and improve the load capacity of the manipulator, spiral bevel gear system should be used. In this case, the bevel train should meet some specific assembly conditions to ensure this mechanism work normally, like the same modulus and pressure angle of each bevel gear, the opposite handedness between the central gear and other gears, the same teeth of the swing-limb gears, and so on. When its end effector is working, the central bevel gear is locked, only the three prismatic pairs provide the motions for the mechanism, which can determine specific kinematics, workspace, and stiffness mapping. When different workspace and stiffness mapping are required, the bevel gear system can adjust the displacement of sliders, then the basic structural parameters of the mechanism

https://doi.org/10.1017/S0263574717000236 Published online by Cambridge University Press

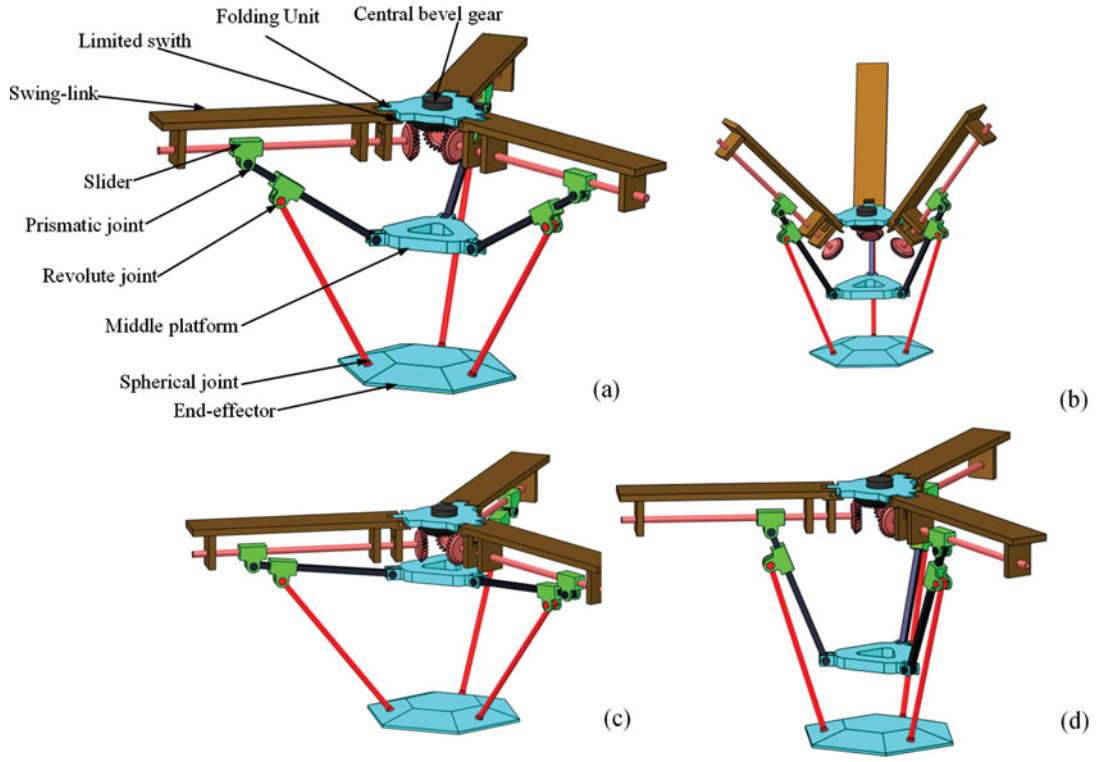


Fig. 1. Three-DOF reconfigurable parallel mechanism: (a) generic configuration, (b) folding pattern, (c) reconfigurable pattern-1, (d) reconfigurable pattern-2.

will be changed. The other advantage of the mechanism is the folding unit. The base platform of the parallel mechanism is not fixed, i.e., it consists of three swing links and the central platform. Due to the inherent design of the mechanism, the fixed platform can be folded when it is necessary, e.g., when installing and disassembling the mechanism.

2.2. Mobility analysis

The mechanism consists of two sections. The mobility of hybrid mechanism is one DOF, and the parallel mechanism has three DOF calculated as follow. When the parallel section is in a certain location, the moving platform and three decline linkages can be considered as a rigid. So, there are eight links, three revolute joints, three prismatic joints, and three spherical joints. Hence, the DOF of the parallel mechanism can be obtained by the Chebychev–Grübler–Kutzbach equation.

$$F = \lambda\,(n - j - 1) + \sum_{i=1} f_i = 3 \tag{1}$$

where λ is the motion parameter, n is the number of links, j is the number of joints, and f_i is the degrees of relative motion permitted by joint i. Overall, the whole DOF is four (plus the one-DOF hybrid mechanism).

A schematic model has been constructed and illustrated in Fig. 2. As shown in Fig. 2, the parallel section can be simplified into a simple 3-PRS parallel mechanism, which has two platforms including the fixed platform and end effector. The original O is attached to the ground and is represented by the coordinates $[\,x\ y\ z\,]$ in which $x-$axis is aligned with the XO, while the end effector has a local original O_1, with coordinates$[\,x_1\ y_1\ z_1\,]$ where $x-$axis is coincident with the line O_1D_1.

The following parameters define the details of the structure:

- r_1 and r_2 are the radiuses of the middle platform and end effector, respectively.
- l_i is the length of the active link.
- θ is the angle between the actuators and the base platform.

https://doi.org/10.1017/S0263574717000236 Published online by Cambridge University Press

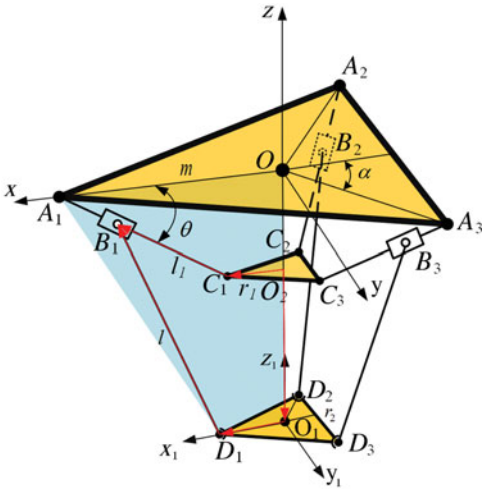


Fig. 2. Simplified schematic diagram of three-DOF parallel mechanism.

The simplified schematic diagram of the reconfigurable section is shown in Fig. 3. The displacement between original point and middle platform is denoted by h, which is actuated by the gear train system. m represents the reconfigurable structural parameter. The relationship among reconfigurable parameter θ, system parameters r_1 and h can be derived by Eq. (2) from Fig. 3

$$h = (m - r_1) \cdot \tan(\theta) \tag{2}$$

The orientation of the end effector of O_1 can be denoted by Euler angle $(\theta_x\ \theta_y\ \theta_z)$. Then, the rotation matrix can be obtained as follows:

$$\begin{aligned} T &= R(z, \theta_z)\, R\left(y, \theta_y\right) R(x, \theta_x) \\ &= \begin{bmatrix} \cos\theta_z\cos\theta_y & \cos\theta_z\sin\theta_y\sin\theta_x - \sin\theta_z\cos\theta_x & \cos\theta_z\sin\theta_y\cos\theta_x + \sin\theta_z\sin\theta_x \\ \cos\theta_y\sin\theta_z & \cos\theta_x\cos\theta_z + \sin\theta_x\sin\theta_y\sin\theta_z & \cos\theta_x\sin\theta_y\sin\theta_z - \cos\theta_z\sin\theta_x \\ -\sin\theta_y & \cos\theta_y\sin\theta_x & \cos\theta_x\cos\theta_y \end{bmatrix} \end{aligned} \tag{3}$$

The relationship between fixed and moving coordinate systems is

$$D_i = TD_{iO_1} + O_1 \tag{4}$$

where D_i is the vector in the fixed coordinate and D_{iO_1} is in the end effector.

As shown in Fig. 2, the coordinates of each point in the end effector are

$$D_{1O_i} = \begin{bmatrix} a_i r_2 & b_i r_2 & 0 \end{bmatrix}^T, \quad O_1 = \begin{bmatrix} x_1 & y_1 & z_1 \end{bmatrix}^T \ (i = 1, 2, 3)$$

Substituting into Eq. (4) yields

$$D_i = \begin{bmatrix} x_1 + a_{x_i} r_2 \cos\theta_y \cos\theta_z + b_{x_i} \cos\theta_x \sin\theta_z + c_{x_i} \cos\theta_z \sin\theta_x \sin\theta_y \\ y_1 + a_{y_i} r_2 \cos\theta_y \cos\theta_z + b_{y_i} \cos\theta_x \sin\theta_z + c_{y_i} \cos\theta_z \sin\theta_x \sin\theta_y \\ z_1 + a_{z_i} \sin\theta_y + b_{z_i} \cos\theta_y \sin\theta_x \end{bmatrix} (i = 1, 2, 3) \tag{5}$$

where the a_{xi}, b_{xi}, and c_{xi}, respectively, represent the different coefficients, and the detailed results have been shown in appendix A.

In this paper, the mechanism is driven by four actuators, while the pose of the parallel mechanism is determined by three actuators. That is, the end effector only has three DOFs, so the six parameters of the position and orientation should be coupled. In this case, the three independent parameters should be calculated. In this case, when the end effector is located at a point, the pose is determined. This

https://doi.org/10.1017/S0263574717000236 Published online by Cambridge University Press

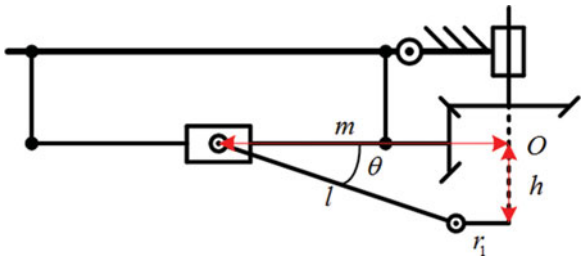


Fig. 3. Simplified schematic diagram of reconfigurable section.

section is to obtain the independent parameters from six parameters represented by x_1, y_1, z_1, θ_x, θ_y, and θ_z. In Fig. 2, the limb $OA_1B_1D_1O$, is in one plane which is rendered by light blue, and other limbs, $OA_2B_2D_2O$ and $OA_3B_3D_3O$, are also in one plane. According to the location of coordinate system, which gives

$$y_{D_i} = a_{1i}x_{D_i} \tag{6}$$

where y_{D_i} and x_{D_i} represent the y or x in the D_i point of the ith limb separately, and a_{1i} is $\pm\sqrt{3}$.

Substituting Eq. (5) to Eq. (6), the constraint equations can be obtained:

$$\begin{cases} \theta_z = \arctan\left(\frac{\sin\theta_x \sin\theta_y}{\cos\theta_x + \cos\theta_y}\right) \\ y_1 = -r_2\left(\sin\theta_x \sin\theta_y \cos\theta_z - \cos\theta_x \sin\theta_z\right) \\ x_1 = \frac{r_2\left(\cos\theta_y \cos\theta_z - \sin\theta_x \sin\theta_y \sin\theta_z - \cos\theta_x \cos\theta_z\right)}{2} \end{cases} \tag{7}$$

The motions along the x, y axes and with θ_z axis are passive motions, which the mechanism is determined by three independent parameters, rotation around x, y axes and translation along $z-$axis. So the end effector of the reconfigurable mechanism has three DOFs, including two rotations and one translation. The mobility can be verified by the Eq. (7).

3. Kinematic Analysis

3.1. Forward kinematics

The coordinates of B_i are illustrated in Fig. 2, which are

$$B_i = \left[a_{2_i}(m - l_1\cos\theta)\ b_{2_i}(m - l_2\cos\theta)\ l_i\sin\theta\right]^{\mathrm{T}} (i = 1, 2, 3) \tag{8}$$

To compute the pose of the end effector, the coordinates of D_i should be obtained. From the constrain of the fixed lengths of the link B_iD_i, it could be a forward problem for $D_iB_i = l (i = 1, 2, 3)$.

So the equation set can be obtained as

$$\begin{cases} \left(-m + x_{D_1} + l_1\cos\theta\right)^2 + \left(z_{D_1} - l_1\sin\theta\right)^2 = l^2 \\ \left(x_{D_2} + \frac{m - l_2\cos\theta}{2}\right)^2 + \left(y_{D_2} + \frac{\sqrt{3}(m - l_2\cos\theta)}{2}\right)^2 + \left(z_{D_2} - l_2\sin\theta\right)^2 = l^2 \\ \left(x_{D_3} + \frac{m - l_3\cos\theta}{2}\right)^2 + \left(y_{D_3} - \frac{\sqrt{3}(m - l_3\cos\theta)}{2}\right)^2 + \left(z_{D_3} - l_3\sin\theta\right)^2 = l^2 \end{cases} \tag{9}$$

Substituting Eq. (8) to Eq. (5) yields

$$z_{D_i} = \frac{\pm\sqrt{2}\sqrt{2l^2 - l_i^2 - 2m^2 + 4mx_{D_i} - 2x_{D_i}^2 + 4l_im\cos\theta - 4l_ix_{D_i}\cos\theta - l_i^2\cos 2\theta} + 2l_i\sin\theta}{2} \tag{10}$$

In Eq. (10), z_{D_i} is a function of the coordinate (x_{D_3}) indirectly. And the $\pm$ refers to the two solutions as well. Then, based on the end-effector geometric constraints, another equation set is written

https://doi.org/10.1017/S0263574717000236 Published online by Cambridge University Press

as follows:

$$\begin{cases} \left(x_{D_3} - x_{D_1}\right)^2 + \left(y_{D_3} - y_{D_1}\right)^2 + \left(z_{D_3} - z_{D_1}\right)^2 = 3r_2^2 \\ \left(x_{D_3} - x_{D_2}\right)^2 + \left(y_{D_3} - y_{D_2}\right)^2 + \left(z_{D_3} - z_{D_2}\right)^2 = 3r_2^2 \\ \left(x_{D_2} - x_{D_1}\right)^2 + \left(y_{D_2} - y_{D_1}\right)^2 + \left(z_{D_2} - z_{D_1}\right)^2 = 3r_2^2 \end{cases} \tag{11}$$

Substituting Eqs. (6) and (10) to Eq. (11) yields x_{D_1}, and the coordinates of D_i can be solved through Eqs. (6) and (10) directly. However, it is difficult to solve the analytical solution of the forward kinematics. In general, numerical solution is applied. Finally, the position coordinate of the center point located in the end effector can be written as follows:

$$O_1 = \left[\frac{\sum_{i=1}^{3} x_{D_i}}{3} \ \frac{\sum_{i=1}^{3} y_{D_i}}{3} \ \frac{\sum_{i=1}^{3} z_{D_i}}{3} \right]^{\mathrm{T}} \tag{12}$$

While the vector of the end-effector orientation can be obtained as follows:

$$\vec{n} = \overrightarrow{D_1 D_2} \times \overrightarrow{D_2 D_3} \tag{13}$$

3.2. Inverse kinematics

The loop closure equation is given by (for $i = 1, 2, 3$)

$$\overrightarrow{O_2 O_1} + \overrightarrow{O_1 D_i} + \overrightarrow{D_i B_i} = \overrightarrow{O_2 C_i} + \overrightarrow{C_i B_i} \tag{14}$$

Based on the parallel mechanism structure in Fig. 2, the vectors of right side of the Eq. (14) can be written as

$$\overrightarrow{O_2 B_i} = \left[a_{3_i}(r_1 + \cos\theta l_i) \ b_{3_i} \ (r_1 + \cos\theta l_2) \ h - \sin\theta l_1 \right]^{\mathrm{T}} (i = 1, 2, 3) \tag{15}$$

From the constrain of the fixed length of the links $D_i B_i$, the following equations can be derived:

$$D_i B_i = l \quad (i = 1, 2, 3) \tag{16}$$

Substituting Eqs. (5) and (15) to Eq. (16), the $l_i (i = 1, 2, 3)$ can be obtained.

In order to verify the correctness of the kinematics analysis, the trajectory equations of the end effector are given with the industrial application. The mechanism is expected to machine a circular arc in a plane, and the equations can be given as

$$\begin{cases} \theta_x = \cos(0.5t) \\ \theta_y = \sin(0.5t) \\ z = c \end{cases} \tag{17}$$

where t represents time and c is a constant.

In this case, the simulation time is 5 s. Based on the kinematics analysis and simulation software, the results are shown in Fig. 4. In Fig. 4(a), the blue line represents the trajectory of end effector, which is obtained by kinematics analysis, while the red one is obtained by the simulation software. Their shapes are similar, and the difference is the rotation angle of the curves, which is caused by the direction of the coordinate system. The Fig. 4(b) and (c) show the variation trends of three prismatic joints obtained from the two ways. The former shows that the lengths' variations of different prismatic joints calculated by kinematics analysis, and the later shows that the displacements of the corresponding joints. Although the former and later y-axis are different, their variation trends are similar. As a result, the correctness of the kinematics analysis can be verified.

https://doi.org/10.1017/S0263574717000236 Published online by Cambridge University Press

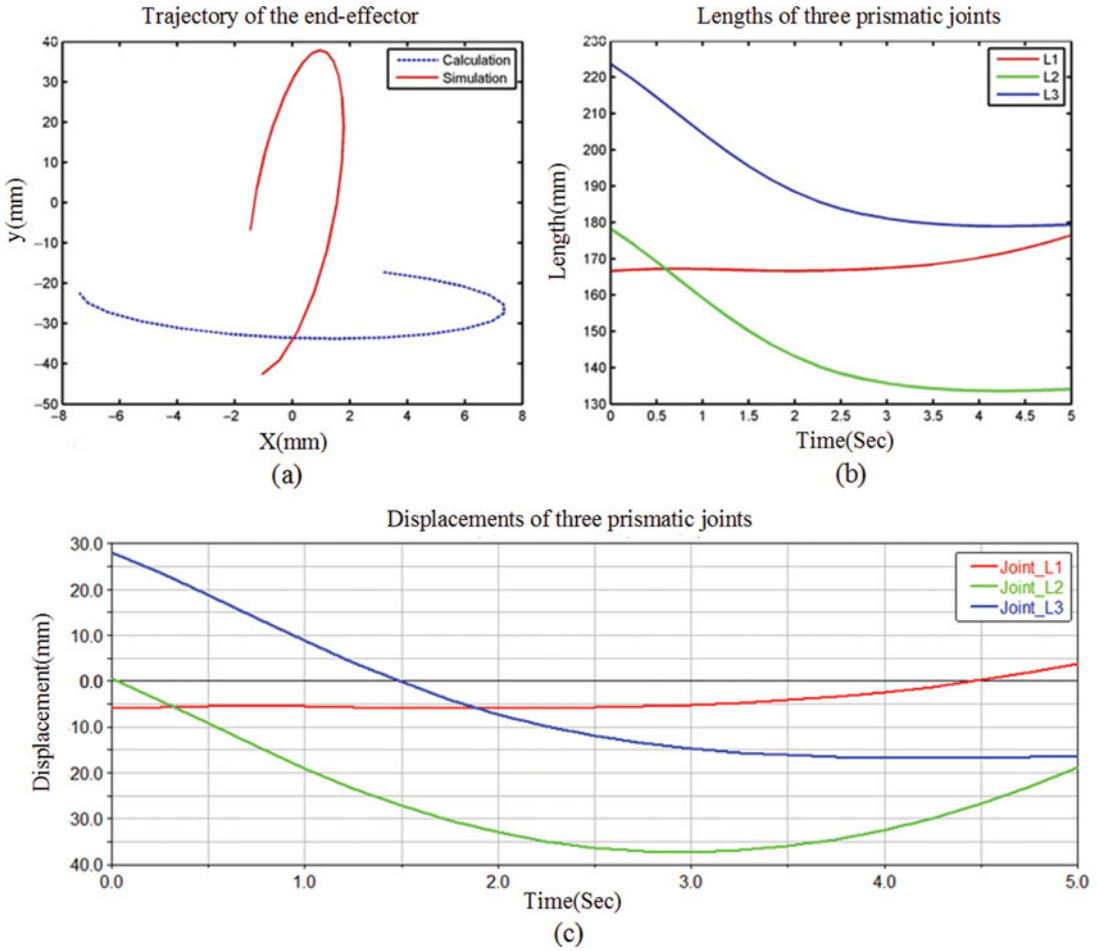


Fig. 4. Comparison between calculation and simulation: (a) the trajectory comparsion between calculation and simulation, (b) the lengths obtained from theoretical analysis, (c) the displacements obtained from simulation.

3.3. Jacobian formulation

The Jacobian analysis of a parallel mechanism is traditionally formulated directly from the time derivative of the vector loop equation. It can be defined as matrix of all first-order partial derivatives of a vector-valued function, in which the motions of the parallel mechanism are represented by the independent joints. In this paper, the proposed parallel mechanism works at a particular configuration, which means the reconfigurable section is locked when the mechanism is working. In this case, the Jacobian matrix is only calculated for the parallel section. Taking the time derivative of Eq. (9) yields

$$\begin{bmatrix} \delta x \\ \delta y \\ \delta z \end{bmatrix} = [J_x] \begin{bmatrix} \partial \theta_x \\ \partial \theta_y \\ \partial p_z \end{bmatrix} \tag{18}$$

where J_x is denoted as the inverse Jacobian matrix, simply, J_x is

$$J_x = \begin{bmatrix} J_{x11} & J_{x12} & J_{x13} \\ J_{x21} & J_{x22} & J_{x23} \\ J_{x31} & J_{x32} & J_{x33} \end{bmatrix} \tag{19}$$

https://doi.org/10.1017/S0263574717000236 Published online by Cambridge University Press

Differentiating the constraint equation to driving variables yields

$$J_q = \begin{bmatrix} J_{q\,11} & 0 & 0 \\ 0 & J_{q\,22} & 0 \\ 0 & 0 & J_{q\,33} \end{bmatrix} \tag{20}$$

where J_q is denoted as the forward Jacobian matrix. Thus, the Jacobian matrix can be calculated as follows:

$$J = {J_q}^{-1} \cdot J_x \tag{21}$$

As a result, the relationship between movement and input parameters can be found.

4. Performance Analysis

4.1. Workspace

For the parallel mechanism, the shape and size of the reachable workspace of the end effector is defined as the space that can be reached by the end effector in the fixed reference frame. The basic constraints that limit the workspace include the moving ranges, component interference, and geometric constraints of the joints in the limb.[29–31]

The actuator's stroke is one of the factors that restrain the workspace of the end effector. Based on the mechanism design, the physical possibilities of the length of the prismatic actuators consist of minimum and maximum values. So the corresponding constraints of each limb are given by

$$l_{i\ \min} \leq l_i \leq l_{i\ \max} \tag{22}$$

where $l_{i\ \min}$ and $l_{i\ \max}$ are the minimum and maximum values of the actuated length of each limb.

As shown in Fig. 5, the workspace of the parallel mechanism is significantly affected by angles β and δ. In order to get the *safe working zone,*[29] both joint limits and singularity should be considered. In this case, the singular constraint can be written as

$$\mathrm{Det}\,(J_i) \neq 0\,(i = 1, 2, 3 \cdots n) \tag{23}$$

where i represents the points in the workspace.

The angle between end effector and the actuated limb can be denoted β, and the range of β is also limited to be within proper range. The angle β represents the spherical joint attached to the end effector is the major critical angular joints. And the range of β depends mainly on the chosen size of the mechanism. In this paper, the angular constraint can be written as the following relationship:

$$\beta_i = \arccos \frac{\overrightarrow{B_i D_i} \cdot \overrightarrow{D_i O_2}}{\overrightarrow{B_i D_i} \cdot \overrightarrow{D_i O_2}} (i = 1, 2, 3) \tag{24}$$

The β_i is constrained by

$$\beta_{i\ \min} \leq \beta_i \leq \beta_{i\ \max} \tag{25}$$

where $\beta_{i\ \min}$ and $\beta_{i\ \max}$ are the minimum and maximum values between the actuated limb and the end effector.

In order to work normally, the range of the passive joint variable, δ, is also constrained within a certain range. Generally, the angle depends on the size of the structural parameters. Thus, the equation can be given as

$$\delta_{\min} < \arccos \frac{\overrightarrow{B_i D_i} \cdot \overrightarrow{B_i C_i}}{\left\|\overrightarrow{B_i D_i}\right\| \cdot \left\|\overrightarrow{B_i C_i}\right\|} < \delta_{\max} \tag{26}$$

https://doi.org/10.1017/S0263574717000236 Published online by Cambridge University Press

Table I. The structural parameters of the mechanism.

Parameter	Value	Parameter	Value
r_1	50	$\boldsymbol{l}_{i\min}$	10
r_2	40	$\boldsymbol{l}_{i\max}$	80
M	112	$\beta_{i\ \mathbf{min}}$	30°
θ	24°	$\beta_{i\ \mathbf{max}}$	120°
l	90		

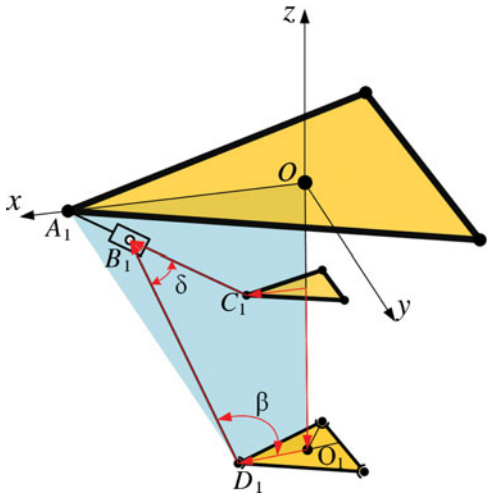


Fig. 5. Schematic diagram of joint limits.

All the limitations are encoded directly into the workspace calculation for a more accurate representation.

In this section, the workspace in the Cartesian coordinate system is calculated and the numerical result is presented.

Especially, the structural parameters and the related values of all joints' moving ranges are utilized as the numerical example for the workspace calculation as listed in the Table I. The step size of $z-$axis chosen for illustration is 1 mm, and the division value of the angle θ_x and θ_y are both 0.01π. In this way, both accurate and computation time are to be guaranteed.

Figure 6 shows the Cartesian workspace of the parallel mechanism with the specific parameters listed in Table I. As shown in Fig. 6, the overall workspace and the mechanism are both drawn in the Cartesian coordinate sysytem. From the comparison between the workspace and mechanism, the workspace can satisfy the requirements of mechanical processing tasks. The planes xoy and yoz are illustrated in Figs. 7 and 8, respectively. As illustrated in Table II, the workspace is symmetrical and the boundaries of the reachable workspace are $x \in [-20, 20]$, $y \in [-18, 18]$, $z \in [-14, 85]$ (the unit is mm). By analyzing these figures, some conclusions can be obtained as follows:

1. The $x - y$ section has different shapes and size with the change of the value z.
2. When the value of z is between 20 mm and 50 mm, the mechanism has the better performance in terms of workspace.
3. When the value of z is above 50 mm, limited by the structure of the mechanism, the available workspace is declining rapidly. Generally, the workspcae of the mechanism meets the requirement very well.

4.2. Stiffness modeling

The stiffness of a mechanism is affected by many factors, e.g., the material of the mechanism, the end-effector position and orientation, and the structure of the limb. For the parallel mechanism, its stiffness refers to the output of the end effector in the working process. Essentially, the static problem is to find the relationship between the input stiffness of the actuators and the output stiffness of the

https://doi.org/10.1017/S0263574717000236 Published online by Cambridge University Press

Table II. The extreme values of the reachable workspace.

Orientation	Minimum value	Maximum value
x	−20 mm	20 mm
Y	−18 mm	18 mm
z	14 mm	85 mm

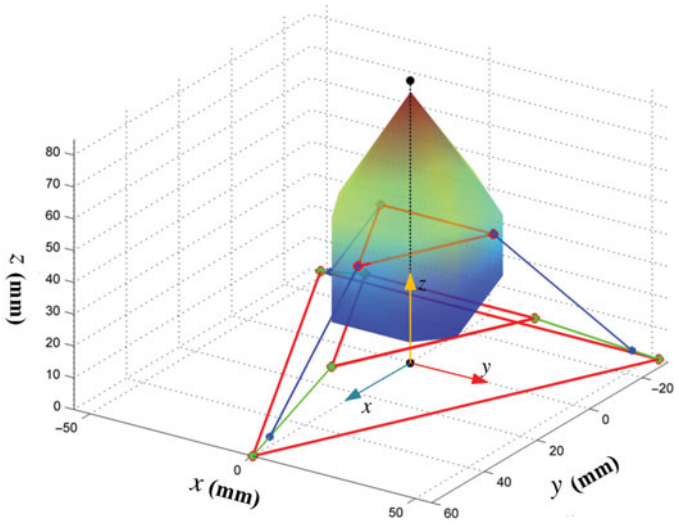


Fig. 6. End-effector workspace.

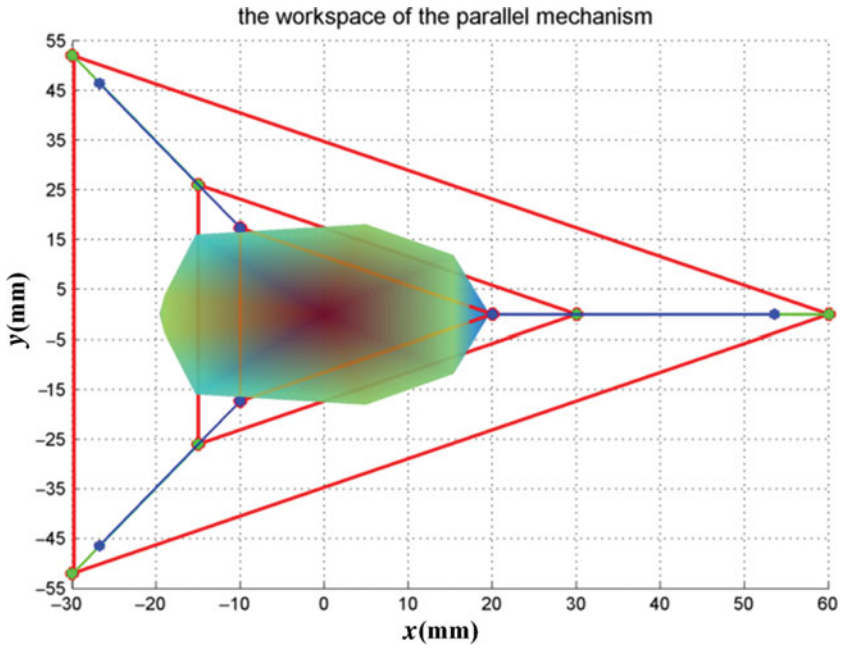


Fig. 7. xoy projection of the workspace.

end effector.To simplify this problem, the joints and links of this system are assumed to be a rigid. The stiffness related to a wrench acting on the end effector can be written as

$$\sigma = \chi \Delta q \tag{27}$$

https://doi.org/10.1017/S0263574717000236 Published online by Cambridge University Press

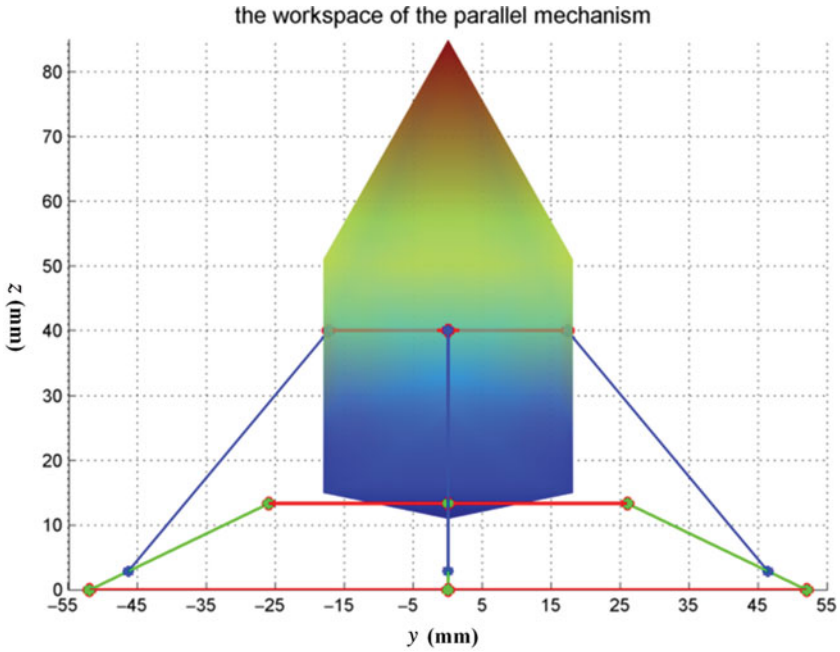


Fig. 8. *zoy* projection of the workspace.

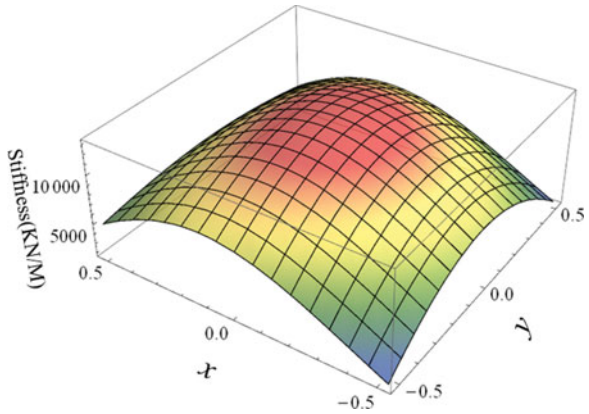


Fig. 9. End-effector stiffness ($z = 50$ mm).

where σ is the wrench vector showing the forces acting on the actuators, which can be represented by $\sigma = [\tau_1, \tau_2, \tau_3]^T$. Δq is the deformation of the corresponding joints, and $\chi = \text{diag}(k_1, k_2, k_3)$ (k_i represents the spring constant). Consequently, the stiffness matrix of the mechanism in Cartesian space is given by the following expression:[32]

$$K = kJ^T J \tag{28}$$

An example of the stiffness in the z -axis is calculated for a definite height is illustrated in Fig. 9. For this example, the $k = 100\,\text{KN/m}$, and $z = 50$ mm, as shown in Fig. 9, when the end effector is close to the central position, its stiffness reaches the maximum, and its stiffness is decreasing rapidly near the boundaries of the workspace. Figure 10 shows the stiffness of the mechanism with different z. When $z = 80\,\text{mm}$, the end effector reaches the maximum stiffness, and its stiffness is the minimum when $z = 30\,\text{mm}$. Therefore, the best working area is between 30 mm and 60 mm along $z -$ axis.

4.3. Dexterity

Dexterity of the mechanism is an important performance index. The index illustartes the relationship between the accuracy at the end effector and the measurement errors on the actuators. It is obtained

https://doi.org/10.1017/S0263574717000236 Published online by Cambridge University Press

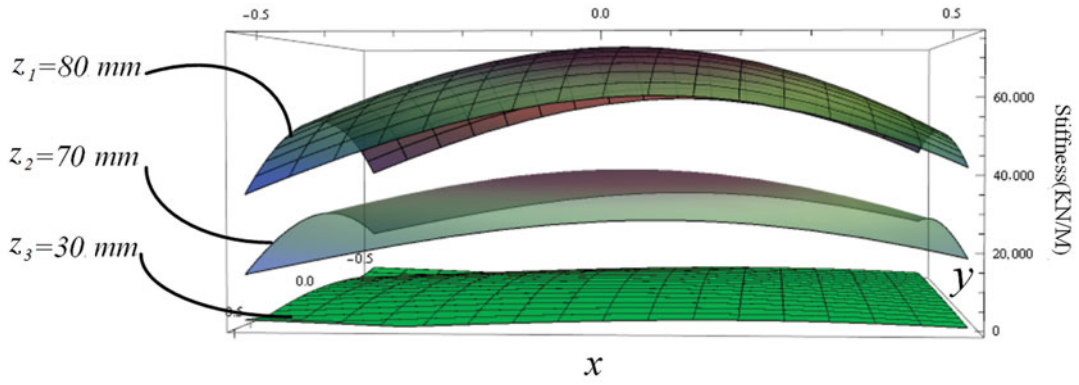


Fig. 10. The stiffness comparison among different z.

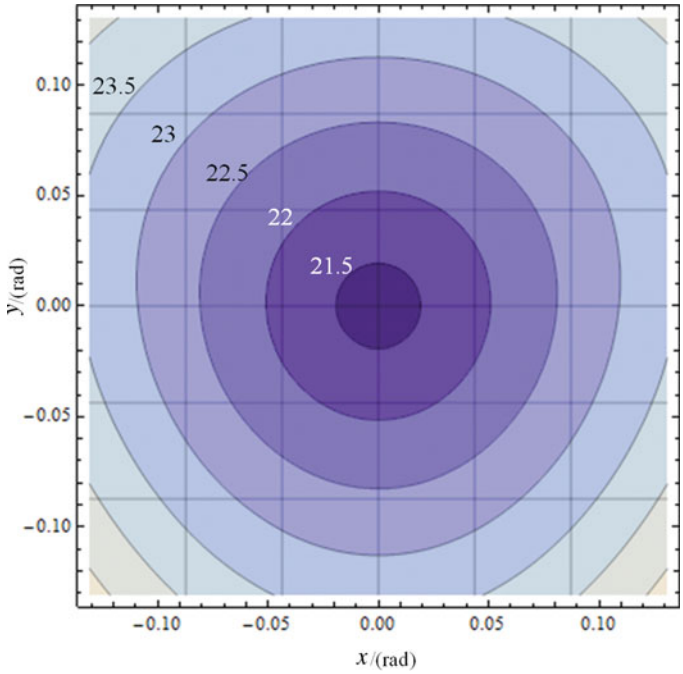


Fig. 11. Jacobian condition number ($z = 50$ mm).

by deriving from Jacobian matrix.[33] Jacobian matrix condition number can be written as

$$\kappa = \|J\| \left\|J^{-1}\right\| \tag{29}$$

The index can be obtained by computing the relation between minimum and maximum eigenvalue of the matrix.[4] i.e.,

$$\kappa = \frac{\sigma_{\max}}{\sigma_{\min}} \tag{30}$$

where $\sigma_{\max}$ and $\sigma_{\min}$ are the largest and the smallest eigenvalues of the Jacobian matrix, respectively. Based on Eq. (29), the dexterity is affected by the location of the end effector. When $\kappa = 1$, the location is called isotropic point, which means the mechanism has the best delivery performance.

The Fig. 11 shows the Jacobian condition number of the mechanism when $z = 50$ mm. From Fig. 11, the mechanism proposed in this paper does not exist isotropic points when $z = 50$ mm. The condition number is distributed symmetrically in plane xoy.

https://doi.org/10.1017/S0263574717000236 Published online by Cambridge University Press

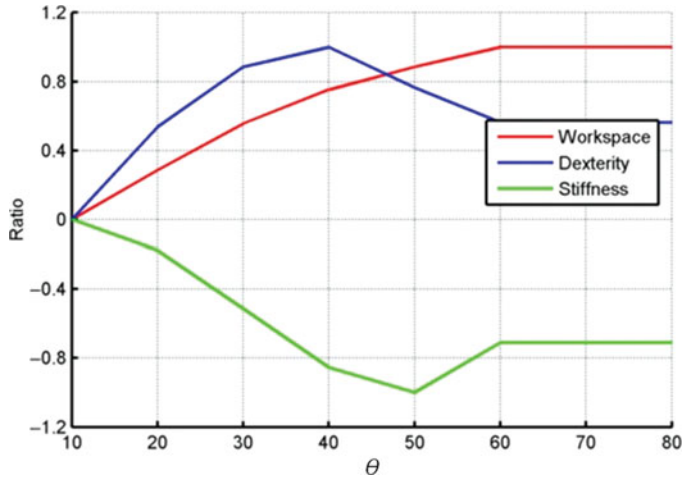


Fig. 12. The trends of performance indexes.

4.4. Comparison

In this paper, the reconfigurable section changes the structural parameters by driving the central bevel gear, namely, changing the angle, θ, which is shown in Fig. 3. When other structural parameters are identical, the performances of the reconfigurable mechanism should be changed with the variation of θ. Therefore, a method is proposed to show the trends clearly. That is,

$$\text{Ratio} = \frac{\text{Index}_i - \text{Index}_1}{\max(\text{Index}) - \min(\text{Index})} \tag{31}$$

In order to ensure that the reconfigurable section work normally, the range of θ is from 10° to 80 °. And, the trends of the performances are shown in Fig. 12. The red, blue, and green lines represent the workspace index, the mean dexterity index, and the mean stiffness index, separately. The workspace of the reconfigurable parallel mechanism increases when the θ is from 10° to 60°. The mean stiffness of the mechanism declines when the θ changes from 10° to 50°. The mean dexterity of the mechanism shows the opposite trend to the stiffness. Both mean stiffness and dexterity keep constant from 60° to 80°.

5. Design Optimization

5.1. Performance criterion

The essential purpose of optimziation is to adjust the geometric dimensions of the mechanism in order to reach better performance.

In this paper, the new design will be used as a machine tool. Therefore, the stiffness, dexterity, and workspace should be in their optimal. In order to evaluate the mechanism's properties within its workspace, comprehensive performance criterion must be proposed. Consequently, the idea of global stiffness index (GSI) is developed. The GSI is the mean stiffness of all the points in the workspace. And the GSI is defined as

$$\text{GSI} = \frac{\int (K)\, \mathrm{d}W}{\int \mathrm{d}W} \tag{32}$$

where

$$\int \mathrm{d}W = \int\int\int \mathrm{d}\theta_x \mathrm{d}\theta_y \mathrm{d}z \tag{33}$$

Meanwhile, as an important performance index of reconfigurable parallel mechanism, the dexterity directly affects the kinematic characteristics. The same like stiffness, the global dexterity index (GDI)

https://doi.org/10.1017/S0263574717000236 Published online by Cambridge University Press

Table III. Variable constraints.

Variable	Constrants	Variable	Constrants
r_1 (mm)	40 50	m (mm)	100 120
r_2 (mm)	30 40	l(mm)	80 100

is defined as the mean dexterity in workspace, which is expressed as

$$\mathrm{GSI} = \frac{\int (\kappa)\, \mathrm{d}W}{\int \mathrm{d}W} \tag{34}$$

Besides the stiffness and dexterity, the workspace is also a significant factor to affect the performance of the parallel mechanism. Ideally, the workspace can be considered as the intensive discrete points and which point has a radius as small as possible, then the workspace can be estimated by the volumes of all the points, so the objective function can be obtained as

$$W = \sum_{i=1}^{n} \frac{4}{3} \pi r_p^3 \tag{35}$$

So these criterion are presented to optimize the performance of the reconfigurable parallel mechanism. For the best kinematics characteristics, the stiffness and workspace should be higher while the value of dexterity should be lower. In order to improve the effective choice, the GSI and GDI are both calculated in the *safe workspace zone.*[29]

5.2. Optimization process

The multi-objective genetic algorithm (MOGA) is applied in this paper. The MOGA is a global search method based on the Darwin's principle of natural selection and genetic modification, which opeartes with a population of possible solutions of the optimization problem. It is a very effective algorithm. Although a single-population genetic algorithm is effective in several situations, the multi-subpopulation evolutionary algorithm can conduct the genetic operation in different populations with a parallel manner, to enhance convergent precision and to deal with more complicated scenarios.[34]

In the process of optimization, the variable parameters are r_1, r_2, m, l. And the variable constraints are listed in Table III. Then, the parameters of proposed optimization method are set as follows: population = 20, array element = 7, front number = 1, crossover probaility = 0.9, mutation probaility = 0.05. The optimization process terminates at maximal generations of 50. Then, the detailed optimization process of multi-objective performances with a Pareto-based MOGA is displayed in Fig. 13.

Table IV shows the results of multi-objective (i.e., GSI,SDI, and workspace) optimization for the structural parameters. Table V shows the 20 sets of objective functions that are chosen for consideration of decision maker. In addition, the order of the related objective values aligns with the order of structural parameters.

To choose the best solution from the 20 sets, a comprehensive index (CI) should be presented to evalute the performance of all solutions. In this paper, since the GSI is generally in the 10^{11} scale and the GDI and workspace are in the 10^0 and 10^2 scales, respectively, the variable weights should be chosen to reflect the comprehensive performance. In this case, the weights of GSI, GDI, and workspace are 10^{-11}, 1, and 10^{-2}, respectively. In order to eliminate effect caused by the scales of these indexes, the indexes are multiplied by special weights. So the CI is developed as follows:

$$\mathrm{CI}_i = w_1 \mathrm{GSI}_i + w_2 \mathrm{GDI}_i + w_3\ \mathrm{Workspace_i}\ (i = 1, 2, \ldots, 20) \tag{36}$$

where w_i is the weight of different objective functions. By comparing the CI value of the objective values from Table V, it can be found the second group in Table IV is the best solution. And the CI values list in Table VI.

https://doi.org/10.1017/S0263574717000236 Published online by Cambridge University Press

Table IV. Optimized design variables.

Number	r_1	r_2	m	l	Number	r_1	r_2	m	l
1	39.26	30.06	125.46	80.07	11	38.95	34.40	142.65	81.49
2	38.49	32.90	110	89.34	12	36.81	34.60	125.78	88.10
3	34.46	30.04	147.04	83.34	13	38.16	32.81	114.24	89.35
4	37.18	35.00	118.18	90	14	37.16	35	118.25	89.97
5	34.25	32.92	150	90	15	39.27	30.00	125.23	80.72
6	39.29	30.11	128.95	80	16	36.49	34.26	123.37	87.40
7	36.89	34.90	125.99	90	17	34.05	32.85	149.61	89.56
8	34.49	32.85	149.05	88.57	18	34.51	32.79	148.41	88.79
9	34.29	30.25	144.18	84.05	19	39.03	34.46	142.62	81.97
10	36.64	30.42	121.07	86.16	20	36.54	34.26	123.19	86.94

Table V. Objective values from the pareto frontier set.

Number	GSI ($\times 10^{11}$)	GDI	Workspace	Number	GSI ($\times 10^{11}$)	GDI	Workspace
1	3.82	4.24	974	11	4.89	4.63	829
2	7.54	7.26	817	12	7.18	6.16	755
3	4.06	3.83	819	13	7.15	6.60	810
4	8.24	7.00	747	14	8.23	6.99	747
5	6.617	5.28	667	15	3.94	4.33	869
6	3.76	4.16	869	16	6.87	6.05	781
7	7.98	6.63	728	17	6.46	5.20	675
8	6.16	5.06	692	18	6.22	5.11	692
9	4.31	4.05	811	19	5.03	4.73	827
10	5.42	5.55	839	20	6.72	5.97	788

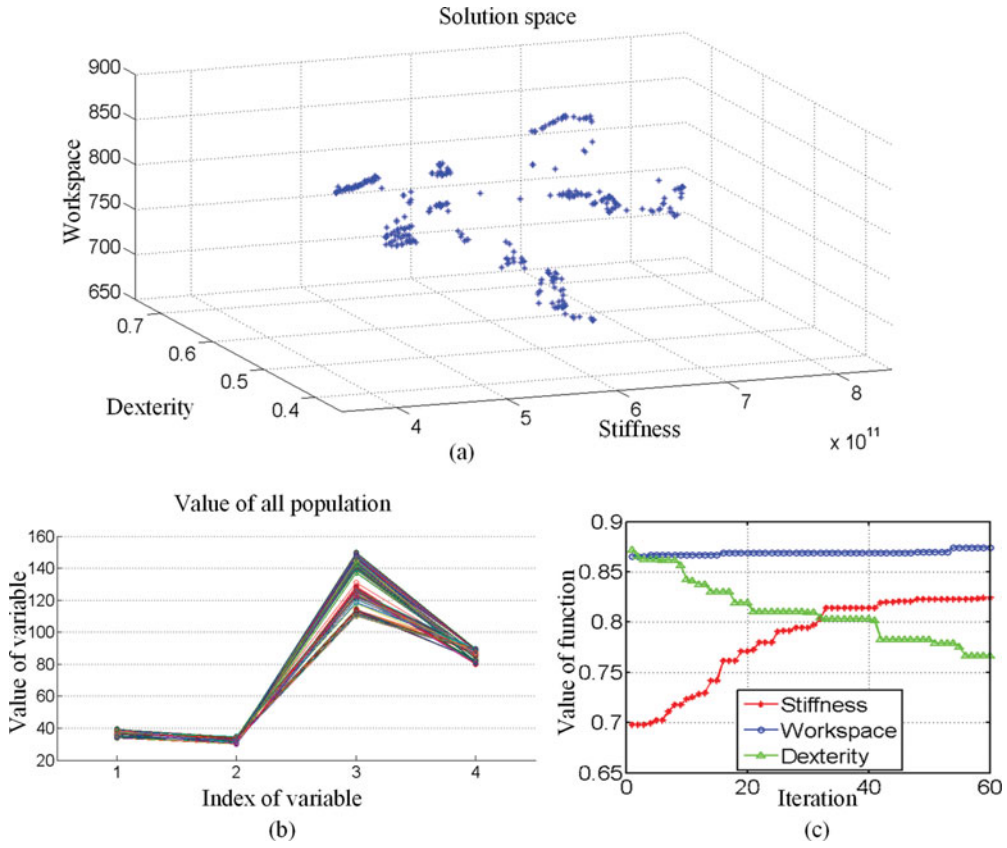


Fig. 13. Multi-objective optimization: (a) Pareto frontier of GSI, GDI, and workspace; (b) variables of all individuals; (c) convergence of objective function.

https://doi.org/10.1017/S0263574717000236 Published online by Cambridge University Press

Table VI. The different valuesof CI.

No.	Value	No.	Value	No.	Value	No.	Value	No.	Value
1	16.80	2	22.98	3	16.09	4	22.72	5	18.57
6	16.62	7	21.89	8	18.14	9	16.48	10	19.37
11	17.82	12	20.89	13	21.85	14	22.70	15	16.96
16	20.74	17	18.41	18	18.25	19	18.04	20	20.57

6. Conclusion

In this paper, a novel reconfigurable parallel mechanism is presented, which can achieve continuous reconfigurable manufacturing purposes by driving a bevel gear system fixed in the base platform. The key property of this mechanism is that it has a bevel gear system which can change the structural parameters, namely, it can reconfigure itself by actuating the bevel gear system. Finally, in order to improve the performances of the parallel mechanism, several performance indices are presented, like GSI, GDIs, and workspace, which influenced the applications. Based on these indices, a multi-objective optimization is applied. Then, taking advantage of the CI, the best structural parameters are selected from the 20 sets of solution. A novel way to select the best structural parameters from the optimized results is introduced in this paper, and this method is generic and can be used for the optimization of the other reconfigurable parallel mechanism.

Acknowledgment

This project is supported by the National Natural Science Foundation of China (NSFC) (Grant No. 51475035, 51505023).

Supplementary Material

To view supplementary material for this article, please visit https://doi.org/10.1017/S0263574717000236.

References

1. Y. Koren, U. Heisel, F. Jovane, T. Moriwaki, G. Pritschow, G. Ulsoy and H. Van Brussel, "Reconfigurable Manufacturing Systems," *CIRP Ann. - Manuf. Technol.* **48**(2), 527–540 (1999).
2. N. Plitea, D. Lese, D. Pisla and C. Vaida, "Structural design and kinematics of a new parallel reconfigurable robot," *Robot. Comput. Integr. Manuf.* **29**(1), 219–235 (2013).
3. A. Moosavian and F. J. Xi, "Design and analysis of reconfigurable parallel robots with enhanced stiffness," *Mech. Mach. Theory* **77**(3), 92–110 (2014).
4. G. Coppola, D. Zhang and K. Liu, "A 6-DOF reconfigurable hybrid parallel manipulator," *Robot. Cim-Int. Manuf.* **30**(2), 99–106 (2014).
5. S. Guo, W. Ye, H. Qu, D. Zhang and Y. Fang, "A serial of novel four degrees of freedom parallel mechanisms with large rotational workspace," *Robotica* **34**(04), 764–776 (2016).
6. X. Kong and C. M. Gosselin, "Type synthesis of 3-DOF translational parallel manipulators based on screw theory," *J. Mech. Des.* **126**(1), 83–92 (2004).
7. X. Kong, "Reconfiguration analysis of a 3-DOF parallel mechanism using Euler parameter quaternions and algebraic geometry method," *Mech. Mach. Theory* **74**(12), 188–201 (2014).
8. X. Kong, "Type synthesis of single-loop overconstrained 6R spatial mechanisms for circular translation," *J. Mech. Robot.* **6**(4), 1–8 (2014).
9. L. Carbonari, M. Callegari, G. Palmieri and M. C. Palpacelli, "A new class of reconfigurable parallel kinematic machines," *Mech. Mach. Theory* **79**(0), 173–183 (2014).
10. G. Coppola, D. Zhang, K. Liu and Z. Gao, "Design of parallel mechanisms for flexible manufacturing with reconfigurable dynamics," *J. Mech. Des.* **135**(7), 1–10 (2013).
11. W. Ye, Y. Fang, K. Zhang and S. Guo, "A new family of reconfigurable parallel mechanisms with diamond kinematotropic chain," *Mech. Mach. Theory* **74**(12), 1–9 (2014).
12. H. Azulay, M. Mahmoodi, R. Zhao, J. K. Mills and B. Benhabib, "Comparative analysis of a new 3×PPRS parallel kinematic mechanism," *Robot. Comput. Integr. Manuf.* **4**(30), 369–378 (2013).
13. X. Zhang and X. Zhang, "A comparative study of planar 3-RRR and 4-RRR mechanisms with joint clearances," *Robot. Cim-Int. Manuf.* **40**, 24–33 (2016).

https://doi.org/10.1017/S0263574717000236 Published online by Cambridge University Press

14. N. Plitea, A. Szilaghyi and D. Pisla, "Kinematic analysis of a new 5-DOF modular parallel robot for brachytherapy," *Robot. Cim-Int. Manuf.* **31**(0), 70–80 (2015).
15. A. Rezaei and A. Akbarzadeh, "Study on Jacobian, singularity and kinematics sensitivity of the FUM 3-PSP parallel manipulator," *Mech. Mach. Theory* **86**(0), 211–234 (2015).
16. L. Carbonari, M. Callegari, G. Palmieri and M. C. Palpacelli, "A new class of reconfigurable parallel kinematic machines," *Mech. Mach. Theory* **79**(0), 173–183 (2014).
17. R. A. Srivatsan and S. Bandyopadhyay, "On the position kinematic analysis of MaPaMan: A reconfigurable three-degrees-of-freedom spatial parallel manipulator," *Mech. Mach. Theory* **62**, 150–165 (2013).
18. D. Gan, J. S. Dai, J. Dias and L. Seneviratne, "Reconfigurability and unified kinematics modeling of a 3rTPS metamorphic parallel mechanism with perpendicular constraint screws," *Robot. Cim-Int. Manuf.* **29**(4), 121–128 (2013).
19. X. Liu, J. Li and Y. Zhou, "Kinematic optimal design of a 2-degree-of-freedom 3-parallelogram planar parallel manipulator," *Mech. Mach. Theory* **87**(0), 1–17 (2015).
20. D. Zhang, L. Wang, Z. Gao and X. Su, "On performance enhancement of parallel kinematic machine," *J. Intell. Manuf.* **24**(2), 267–276 (2013).
21. F. G. Xie, X. J. Liu and J. S. Wang, "Performance evaluation of redundant parallel manipulators assimilating motion/force transmissibility," *Int. J. Adv. Robot. Syst.* **8**(5), 113–124 (2011).
22. M. Li, T. Huang, J. Mei, X. Zhao, D. G. Chetwynd and S. J. Hu, "Dynamic formulation and performance comparison of the 3-DOF modules of two reconfigurable PKM-the tricept and the TriVariant," *J. Mech. Des.* **127**(6), 1129–1136 (2005).
23. X. L. A. C. Fugui Xie, "Design of a novel 3-DoF parallel kinematic mechanism: Type synthesis and kinematic optimization," *Robotica* **33**(3), 622–637 (2014).
24. Z. Gao, D. Zhang, X. Hu and Y. Ge, "Design, analysis, and stiffness optimization of a three degree of freedom parallel manipulator," *Robotica* **28**(03), 349–357 (2010).
25. X. Liu and J. Wang, "A new methodology for optimal kinematic design of parallel mechanisms," *Mech. Mach. Theory* **42**(9), 1210–1224 (2007).
26. Z. Chi and D. Zhang, "Stiffness optimization of a novel reconfigurable parallel kinematic manipulator," *Robotica* **30**(03), 433–447 (2012).
27. Z. Chi, D. Zhang, L. Xia and Z. Gao, "Multi-objective optimization of stiffness and workspace for a parallel kinematic machine," *Int. J. Mech. Mater. Des.* **9**(3), 281–293 (2013).
28. L. Wang, F. Xi, D. Zhang and M. Verner, "Design optimization and remote manipulation of a tripod," *Int. J. Comput. Integ. M* **18**(1), 85–95 (2005).
29. R. A. Srivatsan and S. Bandyopadhyay, *Determination of the Safe Working Zone of a Parallel Manipulator* (Springer, Netherlands, 2014).
30. Y. Yang and J. F. O'Brien, "A Geometric Approach for the Design of Singularity-Free Parallel Robots," *IEEE International Conference on Robotics & Automation* (2009). Kobe, pp. 1801–1806.
31. D. Chablat, P. Wenger. Moveability and Collision Analysis for Fully-Parallel Manipulators.RoManSy, Jul 1998, Iftomm, pp.1–8, 1998.
32. Z. Gao and D. Zhang, "Design, analysis and fabrication of a multidimensional acceleration sensor based on fully decoupled compliant parallel mechanism," *Sensors Actuators A: Physical* **163**(1), 418–427 (2010).
33. J. Guo, L. Zhao, L. Dong and Z. Sheng, "The analysis on the processing dexterity of a 3-TPT parallel machine tool," *Procedia EngineeringCEIS 2011* **15**, 298–302 (2011).
34. Z. Gao and D. Zhang, "Performance analysis, mapping, and multiobjective optimization of a hybrid robotic machine tool," *IEEE T. Ind. Electron.* **62**(1), 423–433 (2015).

https://doi.org/10.1017/S0263574717000236 Published online by Cambridge University Press